Numerical Assessment of RF Human Exposure in Smart Mobility Communications

Doi: 10.1109/JERM.2020.3009856

Available at: https://ieeexplore.ieee.org/document/9142353

Publication: IEEE Journal of Electromagnetics, RF and Microwaves in Medicine and Biology

Publisher: IEEE

Numerical Assessment of RF Human Exposure in Smart Mobility Communications

Gabriella Tognola, Barbara Masini, *Senior Member IEEE*, Silvia Gallucci, Marta Bonato, *Student Member, IEEE*, Serena Fiocchi, Emma Chiaramello, Marta Parazzini, *Member, IEEE*, and Paolo Ravazzani, *Member, IEEE*

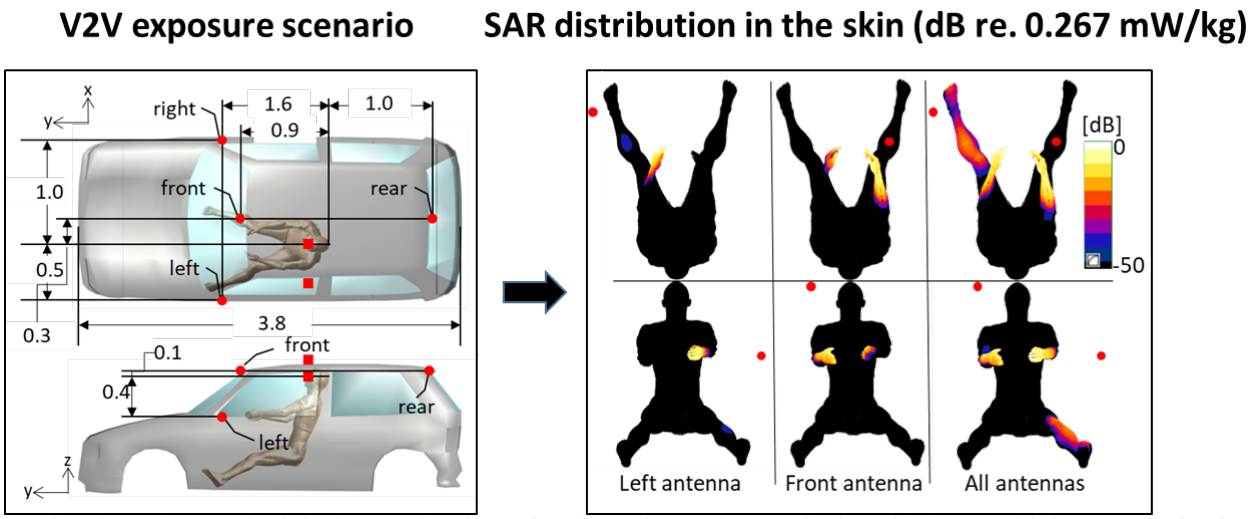

Application of numerical dosimetry for the estimation of SAR in a realistic vehicle-to-vehicle communication scenario.

Take-Home Messages

- Numerical dosimetry was useful to estimate the distribution of EMF in a realistic vehicle-to-vehicle (V2V) communication scenario that includes realistic (for size, dimension, shape and materials) and accurate models of the car, the communicating antennas (four) and a human phantom.
- Specific Absorption Rate (SAR) induced in the worst-case scenario was below the International Commission on Non-Ionizing Radiation Protection (ICNIRP) and IEEE 2019 limits for the general public in the 100 kHz-6 GHz band and was equal to 0.008 W/kg for the whole-body and 1.58 W/kg for local exposure (in the head); in all tested scenarios, the peak of SAR was located in the skin.
- The biological target is the evaluation of SAR in a car passenger (adult driver) due to exposure to 5.9 GHz fields used in V2V communication.
- This work is the first study of RF exposure assessment in the novel scenario of V2V communication and contributes to new and realistic knowledge to assess possible health effects, for the design of policies for public health management.

Numerical Assessment of RF Human Exposure in Smart Mobility Communications

Gabriella Tognola, Barbara Masini, *Senior Member IEEE*, Silvia Gallucci, Marta Bonato, *Student Member, IEEE*, Serena Fiocchi, Emma Chiaramello, Marta Parazzini, *Member, IEEE*, and Paolo Ravazzani, *Member, IEEE*

Abstract Cars are rapidly evolving into smart connected objects that can communicate not only with the infrastructure but also with other cars through vehicle-to vehicle (V2V) communication. By the end of 2023, more than 72 million vehicles worldwide will be equipped with devices and technologies that enable to exchange data and communicate with other cars. This challenging scenario is raising cross-cutting issues, such as those related to new radio-frequency exposures of the human body also when travelling. We evaluate the Specific Absorption Rate (SAR) induced in a realistic smart mobility communication scenario operated at 5.9 GHz. V2V antennas were modeled and placed on a realistic 3D model of a city-car to numerically estimate SAR in the body regions and tissues of a human phantom (adult male) inside the car. We found that both local and whole-body average exposures were below the ICNIRP and IEEE limits for the general public in the 100 kHz-6 GHz band, being equal in the worst case scenario to 1.58 W/kg (head) and 0.008 W/kg, respectively. The highest SAR was found in the most superficial tissues (the skin) of body regions very close to the sources. The distance of the passenger from the antennas played an important role in the resulting SAR. This research has a potentially great clinical impact as it contributes to new and realistic knowledge on the exposure scenario in smart mobility communication to assess possible health effects and for the design of policies for public health management.

Keywords **— Passenger Exposure, smart mobility communication, RF, vehicle-to-vehicle (V2V) antenna, numerical dosimetry**

I. Introduction

CONNECTED vehicles are rapidly changing the way we move, allowing new challenging services and applications for an increased safety, a more efficient traffic management and infotainment. This will be made available by vehicle-to-anything (V2X) communications, which allow vehicles to communicate not only with an infrastructure (V2I), but also directly through vehicle-to vehicle (V2V) communications, with pedestrians (V2P) and the network (V2N). Examples of V2X communications include broadcasting of information for safe mobility (e.g., detection of car accidents, unexpected obstacles, etc.), traffic management, and environment sensing.

Globally, it is predicted that the 70 percent of light-duty vehicles and trucks will be connected to the Internet by 2023 to enhance the driver's experience and provide driver-assistance services, as well as information and entertainment [1]. At present, the automotive manufacturing members of 5GAA (the 5G Automotive Association of companies from the automotive, technology and IT fields for the development of future mobility solutions), operate more than 20 million connected cars that have the ability to connect to cellular networks.

Given this evolving scenario, both the U.S. and Europe are discussing important rules to mandate connectivity on board and foster the penetration of connected cars [2]. In 2016, the U.S. issued a notice of proposed rule-making to mandate V2X communications for all the new light cars, identifying the so-called Wi-Fi for mobility (i.e., IEEE 802.11 p) as the enabling technology, but no decision has been still made about that. In 2019, the European Commission issued a delegated act with the objective to provide the minimal legal requirements to enable large-scale deployment of connected vehicles, promoting ITS-G5 (i.e., the European version of IEEE 802.11p) for short range communications and legacy cellular (3G/4G) for long range. But the Council of the EU objected to the proposal and today, at the best of our knowledge, no mandatory rules have been made available worldwide.

Two are the main wireless access technologies for V2X communications: IEEE 802.11p (or its European version ITS-G5) and Cellular-V2X (C-V2X), both working at 5.9 GHz. The first has been standardized in 2010, tested worldwide with good performance and devices are already available. The second has been standardized in 2017 by 3GPP Release 14 and the first interoperability test have been developed, with good results, in December 2019 [3].

In this work, we focus on IEEE 802.11p, but the model we propose can be extended to C-V2X because, from what concerns the exposure to radio-frequencies, both technologies operate at the same frequencies. As to V2V

All authors are with the Institute of Electronics, Computer and Telecommunication Engineering (IEIIT), CNR, local sites of Milano and Bologna (BM), Italy (e-mail: gabriella.tognola, barbara.masini, silvia.gallucci, marta.bonato, serena.fiocchi, emma.chiaramello, marta.parazzini, paolo.ravazzani@ieiit.cnr.it).

M. Bonato is also with the Department of Electronics, Information and Bioengineering (DEIB), Politecnico di Milano, Italy.

communications, it is worth noting that this technology is leading to novel exposure scenarios with potential impacts not only in the telecommunication field (e.g., for what concerns the management of communication channels and protocols) but also in the health-related field for what concerns the assessment of the exposure of drivers, car passengers and pedestrians to the RF fields generated by these new mobility communication technologies.

To the best of the authors' knowledge, none of the previous studies assessed human exposure in specific V2V communication contexts. V2V exposure has a number of peculiarities that makes it different from other RF exposure scenarios already studied, such as the operating frequency of the sources and the presence of objects (i.e., the metallic body of the car) that might have a significant impact on the distribution of the fields generated by V2V antennas. These peculiarities make impossible to assess RF exposure in V2V communications using the results derived from previous studies. For example, recent studies estimated the RF field generated in realistic V2V scenarios by simulating realistic antennas which were operated at the standard V2V frequency (5.9 GHz) and mounted on realistic car models [4]-[6] These studies didn't assess the exposure on humans as their focus was on the impact of antenna configuration on the performance of the propagation channel. Other recent studies, instead, assessed human exposure to RF in vehicles [7]-[14]. Nevertheless, results from these latter studies are not useful to infer human exposure in V2V scenarios because the sources they investigated (GSM, UMTS, ZigBee, WiMax, and Bluetooth) were operated at frequencies in the 900 MHz-2.5 GHz range that are lower than that used in V2V communication; also RF sources were placed inside the car instead of outside, as in V2V.

The present study applies for the first time a numerical dosimetry approach to specifically assess human exposure in realistic V2V communication conditions, considering realistic sources (V2V antennas) that were operated at the standard V2V communication frequency (5.9 GHz).

II. Methods

A. Antenna, Car, and Human Models

The simulated exposure setup is displayed in Fig.1: it consisted of a human model (adult male) sitting inside a car at the driver position and four antennas placed outside the car, just close to the surface of the car body. At the time of writing there is no indication on which is the best position to place the antennas for vehicular connection. We mounted the antennas at positions that are currently under investigation also by other groups (e.g. [4]-[6]). Antennas are placed symmetrically at the front/rear and left/right sides of the car, namely: close to the left/right mirrors; on the top of the car, near the roof, just close to the windshield ('front' position) and the rear window ('rear' position). Although not a typical montage, we additionally tested a worst case 'asymmetric montage' to evaluate the dose of exposure when the antennas are intentionally placed close to the head (see Fig.1, squared symbols). We thus moved the front antenna over the roof of the car, in a position that stands immediately above the eyes of the driver; the left antenna was moved along the left window and placed at the eyes' height. The right and rear antennas were unchanged. Each antenna was modeled as a quarter-wave monopole with a circular ground plane of one wavelength (λ) of diameter, resembling the dimensions of commercially available antenna modules and were oriented in the $+z$ direction. Similarly to [4]-[6] and in line with the IEEE 802.11p protocol [15], the antennas were operated at 5.9 GHz. The car model, resembling for dimension and shape a typical city car, consisted of a body modeled with a mesh of PEC and six windows modeled as glass (density ρ=2500 kg/m^3; conductivity σ=0.0043 S/m; relative permittivity ε_r=4.82). The interior of the car was filled by air because it was demonstrated [16] that the electric field generated in the car by external or internal sources is only marginally affected by the materials typically used in car interiors, such as foam and thin plastics. The ViP v.1.0 posable Duke human model [17] was used to model a person sitting at the driver position. The model distinguishes nearly 80 different tissues, from the most superficial (e.g., skin) to the most profound ones (e.g., veins, bones). The dielectric properties of Duke's tissues at 5.9 GHz were assigned according to literature data [18]

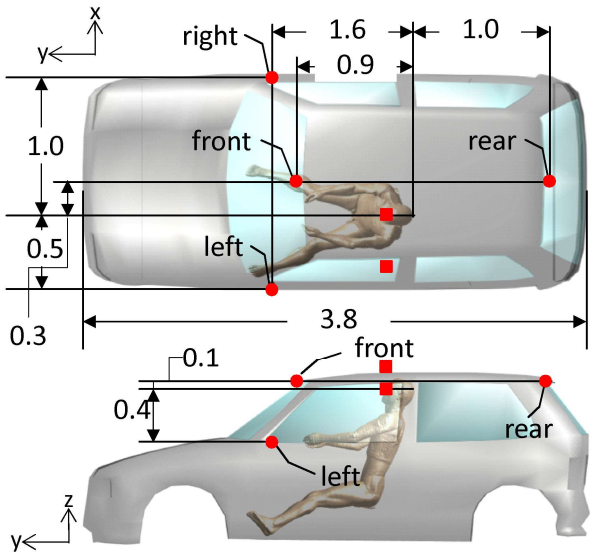

Fig. 1. Top and side view of the exposure setup. The circles show the position of the four antennas (left/right/front/rear) in the 'symmetric montage'. The squares show the position of the front and left antennas in the worst case, 'asymmetric montage' scenario (whereas, right and rear antennas were not changed). Numbers display the dimensions of the car and the distances (m) between the antennas and the driver.

B. Exposure Simulation

Simulations were implemented with the finite-difference time-domain (FDTD) solver of the simulation platform SIM4life (ZMT Zurich Med Tech AG, Zurich, Switzerland, www.zurichmedtech.co). The computational domain included the whole car model, the whole human model and the four antennas. It was discretized with a non-uniform

grid with a maximum step of 2 mm, resulting in a total number of about 10^9 discretization cells. The human phantom was discretized at 1 mm. The simulations converged at the level of -50 dB.

The grid was truncated by assuming a perfectly matched layer (PML) absorbing condition at the domain boundaries which were set at minimum distance of 0.25λ from outer edges of the antennas and the body car. Six different exposure conditions were simulated: five for the 'symmetric montage' (consisting of four single-antenna exposures - one for each antenna - and one with all four antennas simultaneously switched on), and the last one corresponding to the worst case 'asymmetric montage' (all antennas switched on, front and left antennas moved closer to the head). Each antenna was simulated as a 'single edge' voltage source (i.e. as a source which applies an electric field on one single edge on the primary FDTF Yee grid) with an internal reference resistance of 50 Ω. During the post-simulation analysis, the SIM4life software allows to normalize the resulting fields with respect to a target value of the antenna input power, as specified by the user.

C. *Exposure analysis*

We calculated for each of the six exposure conditions the electric field E inside the computational domain and the specific absorption rate (SAR) in the whole body, head, torso, arms, legs, and in all different tissues of Duke. SAR in the whole body (WBS) was computed as the ratio of the total power absorbed in the body to the total mass of the body. For head, torso, arms, and legs, we analyzed the peak of the SAR averaged over any 10 g of the tissues within a given body region ($pSAR_{10gR}$); for tissues, we analyzed both the SAR averaged over 10 g of the tissue (SAR_{10gT}) and its peak value ($pSAR_{10gT}$). To simulate the worst-case exposure, SAR was calculated by assuming an input power of 30 W (EIRP: 44.8 dBm) for each antenna, which corresponds to the maximum allowable input power set by the IEEE 802.11p standard. The input power of 30 W refers to the peak power of the monopole antenna. In all-antenna scenarios, each antenna was operated at 30 W and in phase with the other sources, in order to simulate the worst case scenario.

III. Results

Fig. 2 displays the magnitude of the electric field E generated by the antennas in the typical 'symmetric montage' and evaluated along a line parallel to the ground. The line is placed at the same height of the right and left antennas and intersects the body of Duke at the center of the torso. It can be observed that the electric field generated by the right antenna along the whole evaluation line was negligible. Vice versa, the remaining antennas produced a significant E whose peak values were at the back (for the rear antenna) and the front of the car (for the left and front antennas). Among single-antenna exposures, E generated by the front and rear antennas was the highest because these latter antennas were the closest to the evaluation line. The electric field generated simultaneously by all antennas was concentrated both at the back and the front of the car. The field at the back of the car was the same as that generated by the rear antenna alone. Instead, the field generated by all antennas at the front of the car was higher and distributed over a wider region than that generated by the left, right, and front antennas separately. For all tested exposure conditions, the electric field in the region that intersected the torso of Duke (i.e., the region within the two parallel vertical lines in Fig. 2) was much lower than that observed at the back and the front of the car.

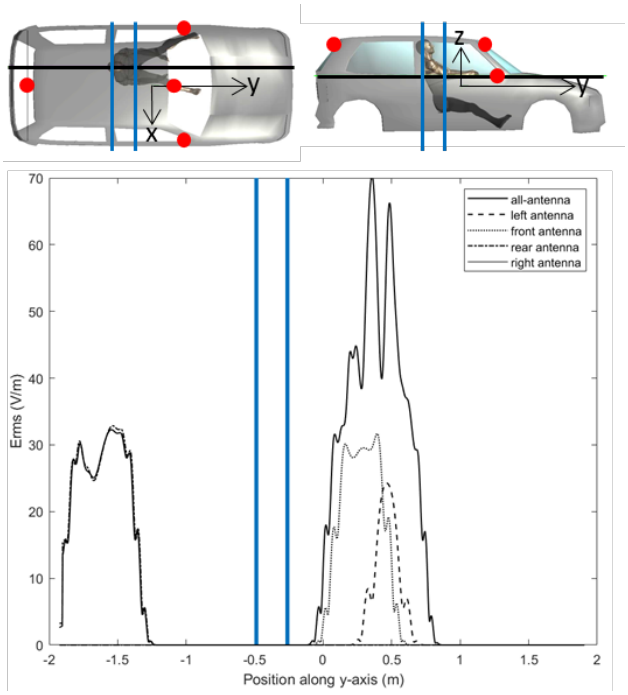

Fig. 2. E field (rms value) generated in single-antenna and all-antenna exposure in the typical 'symmetric montage' and evaluated along a line parallel to the *y*-axis, at *x*=-0.25m, *z*=0.13 m. The miniatures at the top display the position of the evaluation line, the coordinate reference system, the antennas, and the human phantom. The two parallel vertical lines superimposed to the plot of the E field and to the miniatures at the top of the figure delimitate the region along the *y*-axis where the evaluation line intersected the torso of the phantom. The line showing the E field in the 'right antenna' condition is barely visible as the E field is nearly 0.

Table I displays WBS and $pSAR_{10gR}$ induced by each antenna separately and by all four antennas in the 'symmetric' and 'asymmetric' (worst case) configurations. We found that SAR induced by the right and rear antennas alone was negligible (i.e., $<< 10^{-7}$ W/kg) both in the whole body and in every single tissue or body region.

WBS values induced by the front and left antenna separately and by all four antennas simultaneously were not negligible; in all exposure conditions (including the worst case 'asymmetric montage'), WBS was below the 0.08 W/kg limit for the general public exposure in the 100 kHz-6 GHz range set by ICNIRP [19] and IEEE [20]. The highest WBS value, equal to 8.33 mW/kg, was obtained with all four antennas switched on in the worst case 'asymmetric montage'; it decreased to 0.78 mW/kg in the 'symmetric' four-antennas configuration, 0.30 mW/kg with

the front antenna and reached the lowest value (0.19 mW/kg) with the left antenna (both antennas in the 'symmetric montage').

TABLE I
SAR ACROSS DIFFERENT EXPOSURE CONDITIONS

Quantity (mW/kg)	Symmetric montage			Asymmetric montage
	Front antenna	Left antenna	All antennas	All antennas
WBS	0.30	0.19	0.78	8.33
$pSAR_{10gR}$ head	-	-	-	1580.94
$pSAR_{10gR}$ torso	-	-	-	227.45
$pSAR_{10gR}$ left arm	51.20	217.54	266.96	760.63
$pSAR_{10gR}$ right arm	224.94	-	248.58	62.41
$pSAR_{10gR}$ left leg	-	0.63	32.30	7.36
$pSAR_{10gR}$ right leg	-	-	-	-

Mass-averaged whole body (WBS) and peak SAR ($pSAR10_{gR}$) induced in different body regions by the front and left antenna separately and by all four antennas in the 'symmetric montage' and in the worst case 'asymmetric montage'. SAR induced by the right and rear antennas were not displayed as they were negligible ($<<10^{-7}$ W/kg). The symbol '-' stands for 'negligible'.

As to local exposure, $pSAR_{10gR}$ was significant in the limbs in all exposure conditions and in the head and torso in the worst case 'asymmetric montage' scenario, only. The highest $pSAR_{10gR}$ (1580.94 mW/kg) was obtained in the head in the worst case 'asymmetric montage' scenario; in this same scenario, $pSAR_{10gR}$ in the torso was 227.45 mW/kg. As to the limbs, the highest $pSAR_{10gR}$ was observed in the arms and ranged from 51.20 to 760.63 mW/kg across the different scenarios. In the legs, $pSAR_{10gR}$ was much lower than in the arms and negligible in the right leg. In the left leg, it ranged from 0.63 to 32.30 mW/kg, across scenarios. It is to note that in all tested scenarios, $pSAR_{10gR}$ was well below the 4 W/kg limit of local exposure in the 100 kHz-6 GHz range for the limbs set by ICNIRP [19] and IEEE guidelines [20].

As a general remark, SAR in the whole body and the different body regions was higher for all-antenna exposures (for both 'symmetric' and 'asymmetric montage') than for single-antenna exposures. Single-antenna exposures induced significant SAR values only in the nearest body regions, which, according to the exposure setup used in the current simulations (Fig. 1), corresponded to the left and right arms for the frontal antenna and the left arm and leg for the left antenna. Instead, exposure to all four antennas, induced significant SAR values in the arms at both sides, in the left leg and in the head and torso for the 'asymmetric montage' of the antennas.

In all exposure conditions and for all body regions, the highest values of SAR were always observed in the skin. Fig. 3 shows the 3D distribution of the SAR in the skin of Duke across exposure conditions for the 'symmetric montage'. As anticipated in Table I, it is possible to see from Fig. 3 that only the body regions closer to the antennas (i.e., the forearms and the left leg) were characterized by significant SAR values and that in these latter body regions SAR is spread on narrow areas centered at the peak value.

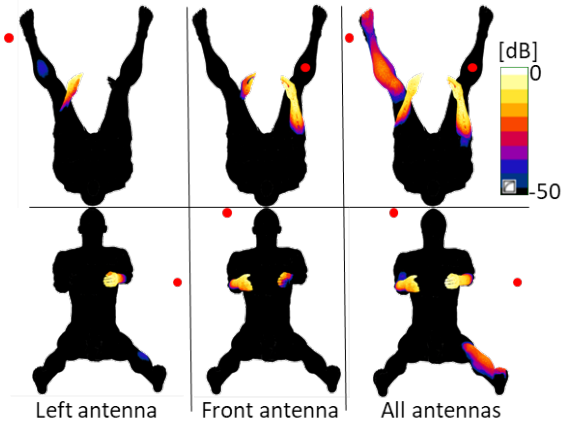

Fig. 3. Top (first row) and fontal view (bottom row) of the 3D distribution of $SAR10_{gT}$ induced in the skin by the left and front antennas separately and by all four antennas simultaneously ('symmetric montage'). SAR values are displayed in dB re. 0.267 mW/kg. The circles indicate the position of the antennas in each exposure condition. To save space in the figure, right and rear antennas were not displayed in the all-antenna condition (rightmost column) as they were far distant from the body of Duke and their contribution to the SAR was negligible.

To further investigate SAR induced in specific tissues, we reported in Fig. 4 SAR_{10gT} and $pSAR_{10gT}$ for the tissues of the left (left column) and right forearm (middle column) and left leg (left column) across exposure condition for the 'symmetric montage'. We found that SAR was significant (i.e., $>>10^{-7}$ W/kg) only in the skin, subcutaneous adipose tissue (SAT), fat, muscles, bones (cortical), and blood. As a general remark, the skin had average SAR_{10gT} and $pSAR_{10gT}$ values much higher than other tissues for all exposure conditions, followed (but to a lower extent) by SAT. For all tissues but blood, exposure to all antennas induced not only higher $pSAR_{10gT}$ than in single-antenna condition but also higher median values and broader distribution of SAR_{10gT}, especially in the skin and SAT. SAR in blood was very small and did not change with exposure condition. The greatest increase in SAR from single- to all-antenna exposure was observed in the tissues of the left forearm and left leg.

Finally, Table II displays $pSAR_{10gT}$ in the tissues of the head, torso, and left arm in the worst case 'asymmetric montage' scenario. It is seen that the head, in particular the skin (1581 mW/kg) and SAT (1530 mW/kg), had the highest SAR. In addition to the skin and SAT, other tissues with high SAR in the head were the eyes, CSF (cerebrospinal fluid), brain, blood, skull, muscles, connective tissues, and the mucosa of the mouth/upper respiratory tract, with $pSAR_{10gT}$ ranging from 1389 mW/kg (mucosa) to 683 mW/kg (blood). Differently from the 'symmetric montage', in this 'asymmetric montage' the torso was exposed to significant dose of RF. However, the tissues of the torso had on average lower SAR values than the head and left arm, which are the body regions closest to the antennas in this latter montage.

TABLE II
SAR IN THE WORST CASE 'ASYMMETRIC MONTAGE' SCENARIO

Tissue	$pSAR_{10gT}$ (mW/kg)
Head	
SAT/skin	1530÷1581
mucosa (mouth, upper respiratory tract)	1389
connective tissue/muscles/skull/ear	1230÷1236
CSF	881
eyes	866
brain	792
blood	683
fat	432
mouth(tongue/teeth)/mandible	179÷190
vertebrae (cervical tract)	54
cerebellum	39
nerves	6
Torso	
thorax bones/SAT/skin	222÷227
muscles/fat	177÷182
larynx	162
trachea/mucosa(respiratory tract)	105
thyroid gland	101
connective tissue	94
blood	36
esophagus	19
vertebrae(dorsal and lumbar tract)/coxae	1÷4
heart/liver/stomach/thymus/spleen/bowels/lung	0.10÷0.72
Left arm	
skin/SAT/muscles	761
bones	610
fat	366
blood	22

Peak SAR ($pSAR10_{gT}$) in the tissues of the head, torso, and left arm induced by all four antennas in the worst case 'asymmetric montage' scenario. For each body region, tissues are arranged in decreasing SAR values. Only tissues with a significant SAR were displayed. Also, SAR in the right arm and left leg was not displayed because it was much lower than that of the 'symmetric montage' (which has been already reported in previous Table I and Fig. 4). CSF: cerebrospinal fluid.

IV. DISCUSSION

This paper presents the first assessment of human RF exposure in realistic V2V communication scenarios. In particular, the present analysis makes use of realistic V2V antennas operated at a frequency which, at the best of the authors' knowledge, has never been studied before.

Our simulations evidenced that the electric field in the car decreased very rapidly with the distance from the antennas; this decrease was much more evident than that usually observed with other mobile and wireless technologies (e.g., GSM, UMTS, WiMax, and Bluetooth) that operate at frequencies (900 MHz-2.5 GHz) lower than in V2V communication (5.9 GHz) and are thus characterized by a lower path loss.

The highest SAR was observed in the very superficial tissues of the body - the skin - and only in body regions at a distance within 0.5 m from the nearest antenna. For the typical 'symmetric montage' of the antennas, SAR was significant only in the limbs and not in the head or torso because in this configuration the head and torso were distant from the antennas. Vice versa, in the 'asymmetric montage' of the antennas (where the front and left antennas were intentionally placed closer to the head/eyes), the head and torso were characterized by significant SAR, in addition to the limbs. In this latter exposure scenario, the head was characterized by the highest SAR which was observed not only in the skin (highest SAR) but also in other tissues such as the eyes, CSF, brain, blood, and skull. For both the 'symmetric' and 'asymmetric montage', local and whole-body average SAR were well below the ICNIRP and IEEE limits for the general public in the 100 kHz-6 GHz band. When compared to single-antenna, exposure to multiple antennas was mainly characterized by an increase of the number of body regions with a significant SAR (both right and left arms and left leg in the multiple-antenna exposure instead of only one arm in the single-antenna exposure) and by a wider spread of SAR over the skin.

Because of the differences in the sources, it is not possible to make a direct comparison with previous studies that assessed human exposure to RF inside vehicles [7]-[14]. It is however interesting to discuss, at least from a qualitative point of view, similarities and differences.

Studies [7] and [8] used FDTD to calculate SAR induced in human phantoms by mobile phones (or similar infotainment RF devices) used inside a car. Leung and colleagues [7] considered a single GSM900 source with a radiation power of 2W. The peak SAR (10 g average) induced in the passenger that is using the phone was much greater than that observed in the driver in our V2V exposure scenario (nearly 3000 mW/kg in [7] instead of 1581 mW/kg in our worst case 'asymmetric montage' scenario). This difference is most probably due to the shorter distance between the source and the person, being lower than 20 mm in [7] and nearly 100 mm in our case. If we consider the exposure of the non-users in [7], the maximum SAR was reported to range from 53 mW/kg to 233 mW/kg, depending on the number of people inside the car. These latter values are of the same magnitude of the SAR we found in our 'symmetric montage' scenario where the peak was 266.96 mW/kg. It is to note that, on average, the distance between the non-users and GSM phone in [7] is comparable to the distance between the driver and the V2V antennas in our 'symmetric montage' scenario.

Harris and colleagues [8] estimated the SAR induced by UMTS, WiMax, and Bluetooth devices operating in the 2.1-2.5 GHz range. WBS obtained in our worst case 'asymmetric montage' exposure was greater than that obtained by [8] in a multiple-source (UMTS+WiMax) exposure condition (8.33 mW/kg instead of 1.28 mW/kg). This is most probably due to the lower power of the sources, being only 125-250 mW in [8] and 30 W in our case. The same trend was observed for localized SAR, which was greater in our case than in [8] (1581 mW/kg in our worst case 'asymmetric montage' scenario instead of 302.2 mW/kg for a single WiMax source exposure condition in [8]).

In [9] and [10], a 3D ray-launching approach was applied to estimate the electric field generated by mobile phones inside a vehicle (car and bus). In [9], the phone (GSM 900) was operated at the maximum power of 2 W and placed at the front desk of the car model. The maximum electric field obtained at the position of the passengers closer to the

phone was 31.89 V/m. In [10], phones (GSM900, GSM1800, and UMTS2100) were positioned in a bus model. The maximum electric field obtained when phones were operated at the maximum power (from 125 mW for UMTS to 2 W for GSM900) ranged from 22 to 54 V/m, depending on the phone frequency band. In our simulations, the electric field generated in the worst case 'asymmetric montage' scenario, when each antenna is switched on and operated at 30 W, ranges from 15 to 30 V/m across the different seat positions in the car (measurements are taken at the torso height). Our values are nearly of the same order of magnitude that in [9] and [10] and correspond to a power density ranging from 0.60 to 2.39 W/m^2, which are below the 10 W/m^2 limits for the general public in the 2-300 GHz band (for exposure time averaged over 30 minutes).

Finally, studies [10]-[14] measured personal exposure in the 900 MHz-2.5 GHz band of people travelling in vehicles. The power density measured experimentally during real car trips typically ranged from 0.25 to 1.9 mW/m^2 across the studies. These values are lower than those obtained in our simulations. One reason of this trend could be that in [10]-[14] measurements were done in real conditions where it is probable that the sources were not operated at the maximum power as in our simulations. In addition, measurements in [10]-[14] were done in non-controlled scenarios where we do not know several important parameters, such as the number of RF sources and the distance of the measurement point from the source. For all these reasons, results from [10]-[14] should be taken only for a qualitatively comparison.

V. Conclusions

In the present study we investigated for the first time the SAR induced inside a car in realistic V2V communication exposure scenarios by using a deterministic numerical dosimetry approach. We analyzed single- and multiple-antenna exposures, also considering a worst-case scenario where antennas were intentionally moved very close to the head of the driver. In all tested exposure scenarios, SAR in the body of the driver was found to be well below the safe limit of current exposure guidelines. Also, exposure decreased very rapidly with the distance from the antennas, being almost negligible at distances greater than 500 mm.

It is important to note that our results were derived in a typical but fixed antenna montage. Therefore, it is crucial to perform further studies to fully to assess V2V exposure with different antenna montages, with more than one people inside the car and also with people of different ages (e.g., adults, children, neonates, fetuses, etc.), for example by using non-deterministic dosimetry approaches, based on Machine Learning or stochastic algorithms [21]-[23]. Last but not least, attention should be given in future studies in determining the impact of mutual antenna coupling on the resulting RF exposure.

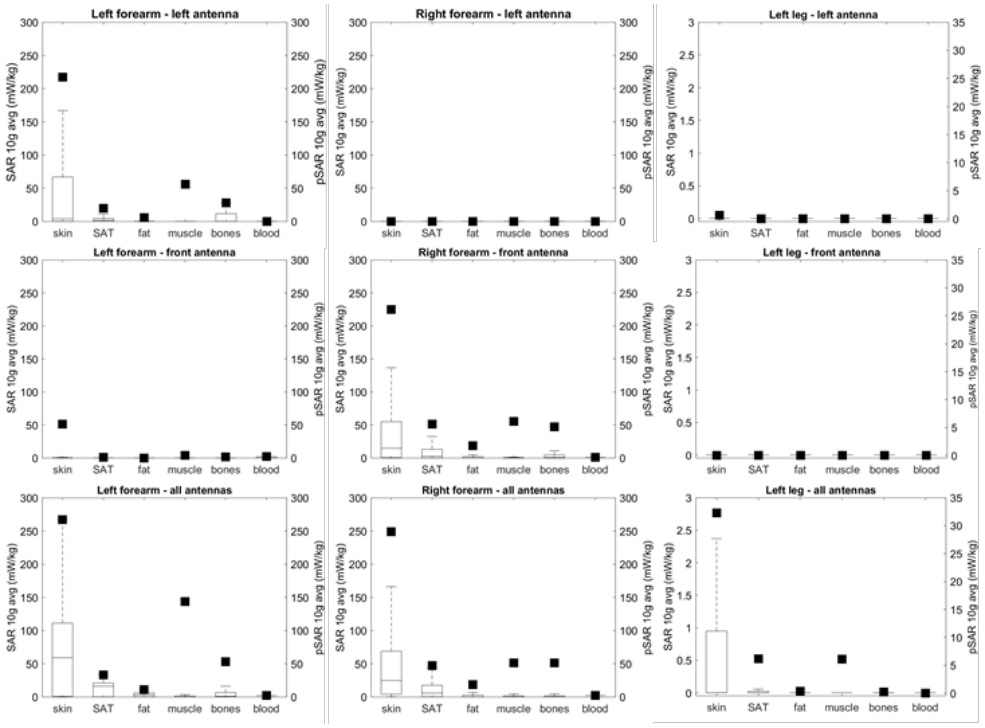

Fig. 4. SAR_{10gT} (left *y*-axis, box plot) and $pSAR_{10gT}$ (right *y*-axis, square symbols) in the tissues of the left forearm, right forearm, and left leg across exposure conditions. SAR_{10gT} and $pSAR_{10gT}$ obtained with the antenna in the rear and right position were not reported as their levels were not relevant (<< 10^{-7} W/kg). The center lines in the boxes indicate the median; the bottom and top edges indicate the 25th and 75th percentiles. The whiskers extend to 1.5 times the height of the box and correspond to approximately 99.3 percent of the data. Differently than in other tissues, SAR_{10gT} of blood in right and left forearms was calculated as the total power absorbed by blood divided by its total mass because the mass of blood in these regions was less than 10 g. Note that scale on the *y*-axes of the plots of the right column (left leg) are zoomed with respect to the other plots.

REFERENCES

[1] Statista, Share of new light-duty vehicles and trucks sold that are connected to the Internet worldwide and in the United States in 202. Available:https://www.statista.com/statistics/275849/number-of-vehicles-connected-to-the-internet/

[2] 5GAA, Roadmap of monetisable features and business models for LTE V2X – timeline for introduction of LTE V2X (V2V), 18 Dec. 2017. Available: https://5gaa.org/wp-content/uploads/2018/10/5GAA_181002_Roadmap-White-Paper.pdf

[3] A. Bazzi, G. Cecchini, M. Menarini, BM. Masini, and A. Zanella, "Survey and perspectives of vehicular Wi-Fi versus sidelink cellular-V2X in the 5G era," *Future Internet*, vol. 11(6), art. no. 122, 2019.

[4] D. Kornek, M. Schack, E. Slottke, O. Klemp, I. Rolfes and T. Kürner, "Effects of antenna characteristics and placements on a Vehicle-to-Vehicle channel scenario," in *Proc. 2010 IEEE International Conference on Communications Workshops*, Capetown, 2010, pp. 1-5.

[5] E. Whalen, A. Elfrgani, C. Reddy and R. Rajan, "Antenna placement optimization for Vehicle-to-Vehicle communications," in *Proc. 2018 IEEE International Symposium on Antennas and Propagation & USNC/URSI National Radio Science Meeting*, Boston, MA, 2018, pp. 1673-1674.

[6] G. Artner, W. Kotterman, G. Del Galdo and M.A. Hein, "Automotive antenna roof for cooperative connected driving," IEEE Access, vol. 7, pp. 20083-20090, 2019.

[7] S-W. Leung, Y. Diao, K-H. Chan, Y-M. Siu, and Y. Wu, "Specific Absorption Rate evaluation for passengers using wireless communication devices inside vehicles with different handedness, passenger counts, and seating locations," *IEEE T Bio Med Eng*, vol. 59, pp. 2905-2912, 2012.

[8] L.-R. Harris, M. Zhadobov, N. Chahat, and R. Sauleau, "Electromagnetic dosimetry for adult and child models within a car: multi-exposure scenarios," *Int J Microw Wirel T*, vol. 3, no. 6, pp. 707–715, 2011.

[9] E. Aguirre, PL. Iturri, L. Azpilicueta, S. De Miguel-Bilbao, V. Ramos, U. Gárate, and F. Falcone, "Analysis of estimation of electromagnetic dosimetric values from non-ionizing radiofrequency fields in conventional road vehicle environments," *Electromagn Biol Med*, vol. 34, pp. 19–28, 2015.

[10] M. Celaya-Echarri, L. Azpilicueta, P. Lopez-Iturri, E. Aguirre, S. De Miguel-Bilbao, V. Ramos, and F. Falcone, "Spatial characterization of personal RF-EMF exposure in public transportation buses," IEEE Access, vol. 7, pp. 33038-33054, 2019.

[11] Z. Judakova and L. Janousek, "Possible health impacts of advanced vehicles wireless technologies," *Transportation Research Procedia,* vol. 40, pp. 1404–1411, 2019.

[12] M. Eeftens, B. Struchen, LE. Birks, E. Cardis, M. Estarlich, MF. Fernandez, P. Gajšek, M. Gallastegi, A. Huss, L. Kheifets, IK. Meder, J. Olsen, M. Torrent, T. Trček, B. Valič, R. Vermeulen, M. Vrijheid, L. van Wel, M. Guxens, and M. Röösli, "Personal exposure to radio-frequency electromagnetic fields in Europe: Is there a generation gap?," *Environ Int*, vol. 121, pp. 216-226, 2018.

[13] S. Sagar, SM. Adem, B. Struchen, SP. Loughran, ME. Brunjes, L. Arangua, MA. Dalvie, RJ. Croft, M. Jerrett, JM. Moskowitz, T. Kuo, and M. Röösli, "Comparison of radiofrequency electromagnetic field exposure levels in different everyday microenvironments in an international context," *Environ Int*, vol. 114, pp. 297-306, 2018.

[14] K. Roser, A. Schoeni, B. Struchen, M. Zahner, M. Eeftens, J. Fröhlich, and M. Röösli, "Personal radiofrequency electromagnetic field exposure measurements in Swiss adolescents," *Environ Int*, vol. 99, pp. 303-314, 2017.

[15] IEEE Standard for Information technology, "Local and metropolitan area networks-- Specific requirements, Part 11: Wireless LAN Medium Access Control (MAC) and Physical Layer (PHY) Specifications Amendment 6: Wireless Access in Vehicular Environments," in *IEEE Std 802.11p*, pp.1-51, 2010.

[16] A. Ruddle, "Influence of dielectric materials on in-vehicle electromagnetic fields," in *Proc. IET Seminar on EM Propagation in Buildings and Large Structures*, London, 2008.

[17] A. Christ, W. Kainz, EG. Hahn, K. Honegger, M. Zefferer, E. Neufeld, W. Rascher, R. Janka, W. Bautz, J. Chen, B. Kiefer, P. Schmitt, HP. Hollenbach, J. Shen, M. Oberle, D. Szczerba, A. Kam, JW. Guag, and N. Kuster, "The Virtual Family—Development of surface-based anatomical models of two adults and two children for dosimetric simulations," *Phys Med Biol*, vol. 55, no. 2, pp. 23–38, 2010.

[18] S. Gabriel, RW. Lau, and C. Gabriel, "The dielectric properties of biological tissues: II. Measurements in the frequency range 10 Hz to 20 GHz", *Phys Med Biol*, vol. 41, pp. 2251-2269, 1996.

[19] International Commission on Non-Ionizing Radiation Protection, "Guidelines for limiting exposure to electromagnetic fields (100 kHz to 300 GHz).", *Health Phys*, vol. 118(5), pp. 483–524, 2020. Pre-print. DOI: 10.1097/HP.0000000000001210.

[20] IEEE International Committee on Electromagnetic Safety, "IEEE Standard for Safety Levels with Respect to Human Exposure to Electric, Magnetic, and Electromagnetic Fields, 0 Hz to 300 GHz," in *IEEE Std C95.1-2019 (Revision of IEEE Std C95.1-2005/ Incorporates IEEE Std C95.1-2019/Cor 1-2019)*, pp.1-312, 4 Oct. 2019.

[21] M. Bonato, E. Chiaramello, S. Fiocchi, G. Tognola, P. Ravazzani, and M. Parazzini, "Influence of low frequency near-field sources position on the assessment of children exposure variability using Stochastic Dosimetry," *IEEE J Electromag RF and Microw Med Biol,* 2019 (Early Access).

[22] G. Tognola, M. Bonato, E. Chiaramello, S. Fiocchi, I. Magne, M. Souques, M. Parazzini, and P. Ravazzani, Use of Machine Learning in the analysis of indoor ELF MF exposure in children", *Int J Environ Res Public Health*, vol. 16, p. 1230-1243, 2019.

[23] G. Tognola, E. Chiaramello, M. Bonato, S. Fiocchi, I. Magne, M. Souques, M. Parazzini, P. Ravazzani, "Cluster Analysis of residential personal exposure to ELF magnetic field in children: effect of environmental variables," *Int J Env Res Public Health*, vol. 16, pp. 4363-4376, 2019.

Gabriella Tognola received the master's degree in electronic engineering and the Ph.D. degree in bioengineering, both from Politecnico di Milano, Milan, Italy. She is currently Senior Research Scientist with the Consiglio Nazionale delle Ricerche, Institute of Electronics, Computer and Telecommunication Engineering. Her main research interests include exposure assessment of electromagnetic fields with numerical dosimetry and with Machine Learning methods and modelling of electromagnetic fields for biomedical applications.

Barbara Masini (S'02-M'05) received the master's degree (summa cum laude) in Telecommunications Engineering and the Ph.D. degree in Electronic, Computer Science, and Telecommunication engineering from the University of Bologna, Italy, in 2001 and 2005, respectively. Since 2005, she is a researcher at the Institute for Electronics and for Information and Telecommunications Engineering (IEIIT), of the National Research Council (CNR). Since 2006 she is also adjunct Professor at the University of Bologna. She works in the area of wireless communication systems and her research interests are mainly focused on connected vehicles, from physical and MAC levels aspects up to applications and field trial implementations.

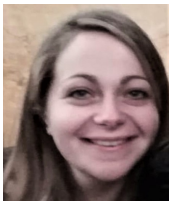

Silvia Gallucci received the master's degree in Biomedical Engineering in 2019 from the University of Pisa (Italy). She currently is currently a research associate at the Consiglio Nazionale delle Ricerche, Institute of Electronics, Computer and Telecommunication Engineering. Her main research interests include exposure assessment of electromagnetic fields with numerical dosimetry, particularly from 5G mobile communications.

Marta Bonato received the master's degree in biomedical engineering from the Polytechnic of Milan, Milan, Italy, in July 2017, where she is currently working toward the Ph.D. degree in bioengineering. From September 2017 to April 2018, she was with the Institute of Electronics, Computer and Telecommunication Engineering, Consiglio Nazionale delle Ricerche, as a Research Fellow. Her research interests are related to the study of the interaction of electromagnetic fields (EMF) with biological systems and the study of possible effects of EMF on health.

Serena Fiocchi received the master's degree in biomedical engineering in 2009 and the Ph.D. degree in bioengineering in 2014, both from the Polytechnic of Milan, Milan, Italy. She is a Research Scientist with the Institute of Electronics, Computer and Telecommunication Engineering, National Research Council of Italy. Her scientific interests include the study of the computational modeling of noninvasive brain and spinal stimulation techniques, the design and the optimization of biomedical technologies based on electromagnetic fields (EMF) for diagnostic and therapeutic applications, and the computational modeling of the interactions between EMF and biological systems.

Emma Chiaramello received the master's and Ph.D. degrees in biomedical engineering from the Politecnico di Torino, Torino, Italy, in 2009 and 2013, respectively. She is a Postdoctoral Research Fellow with the Institute of Electronics, Computer and Telecommunication Engineering, National Research Council of Italy. Her scientific interests include the study of the interactions between EMF and biological systems, with both deterministic dosimetry based on computational electromagnetism methods and stochastic dosimetry based on surrogate modeling.

Marta Parazzini (M'04) is a Research Scientist with the Institute of Electronics, Computer, and Telecommunication Engineering, Italian National Research Council, Milan, Italy. Her primary research interests include the medical applications of EMF, in particular the techniques for noninvasive brain stimulation, the study of the interactions of EMF with biological systems, and deterministic and stochastic computational dosimetry.

Paolo Ravazzani (M'14) received the master's degree in electronic engineering and the Ph.D. degree in bioengineering, both from Politecnico di Milano, Milan, Italy. He is currently Director of the Institute of Electronics, Computer and Telecommunication Engineering of Consiglio Nazionale delle Ricerche. His main research interests include exposure assessment of electromagnetic fields related to the study of the possible effects of electromagnetic fields on health and biomedical applications of electromagnetic fields.